Controlling evolutionary dynamics to optimize microbial bioremediation

Shota Shibasaki and Sara Mitri

Department of Fundamental Microbiology, University of Lausanne, Switzerland

Abstract

Some microbes have a fascinating ability to degrade compounds that are toxic for humans and the environment in a process called bioremediation. Although these traits help microbes survive the toxins, carrying them can be costly if they involve secreting extracellular detoxifying enzymes that benefit all surrounding microbes, whether they detoxify or not. Detoxification can thereby be seen as a public goods game, where non-degrading mutants can sweep through the population and reduce bioremediation efficiency. Here, we constructed an evolutionary game theoretical model to optimize detoxification efficiency in a chemostat initially containing "cooperating" microbes. We consider two types of mutants: "cheaters" that do not detoxify, and mutants that become resistant to the toxin through private mechanisms that do not benefit others. By manipulating the concentration and flow rate of a toxin into the chemostat, we identified conditions where cooperators can exclude cheaters that differ in their private resistance. However, in the long term, cheaters are bound to re-invade. To overcome this inevitable outcome and maximize detoxification efficiency, cooperators can be periodically reintroduced into the population. Our findings highlight the importance of evolutionary dynamics in practical applications, which can equally apply to other toxic environments, such as antibiotic treatments.

Key words: public goods game, evolutionary game theory, eco-evolutionary feedback, chemostat, detoxification

1 Introduction

Microbes can provide a variety of benefits to human society. These include applications ranging from the production of biofuels (Antoni et al., 2007; Lea-Smith and Howe, 2017; Ryan Georgianna and Mayfield, 2012) or other chemicals (Nielsen and Keasling, 2016) to the degradation of toxic compounds (bioremediation) (Bertrand et al., 2015; Mosa et al., 2016; Vidali, 2001), such as heavy metals (Dixit et al., 2015; Kang et al., 2016) or waste water (Chen et al., 2009). In all these applications, the benefits gained from the microbes, in terms of production rates of a given molecule or the efficiency of degradation of a toxic compound, need to maximized. But what is often neglected is another key criterion: the stability of these benefits over time.

There are two ways in which microbial systems can become unstable and lose efficacy. First, if multiple species are used, these ecosystems can be ecologically unstable, whereby the relative abundance of each species changes over time, possibly leading to species extinctions and decreased system performance, as biodiversity can correlate with ecosystem function (Cardinale et al., 2012). Such ecological instabilities can arise due to inter-species interactions, their response to the environment or stochastic events. Second, due to their large population size and short generation times, microbes quickly acquire mutations that can lead to evolutionary instability. Species can thereby lose their ability to perform the ecosystem function (Bull and Barrick, 2017; Kumar et al., 1991). For example, according to a theoretical study, algae are predicted to stop producing biofuels under a constant environment (Akita and Kamo, 2015), and in the lab, engineered *Escherichia coli* lose mevalonic acid production after about 80 generations (Rugbjerg et al., 2018a,b). Similarly, in bioremediation systems, mutants that do not detoxify appear in experimental populations (Ellis et al., 2007; O'Brien et al., 2014). To maximize the functional efficiency of a microbial ecosystem, therefore, we need to consider both ecological and evolutionary dynamics of microbial populations (Schuster et al., 2010).

In this study, we develop a mathematical model to investigate the simple case of a single species degrading a toxic compound in a chemostat and explore its evolutionary stability in the face of mutations, with the goal of optimizing the efficiency of toxin degradation. In our model, we assume that toxins are harmful to the microbes, who degrade them by secreting costly extracellular enzymes. The benefit of degrading toxins is shared by the whole population as our model does not include spatial structure. Toxin degradation can be, therefore, regarded as a public goods game (Samuelson, 1954; Broom et al., 2018), although this term is sometimes defined more loosely in microbiology than in economics (Hummert et al., 2014; Smith and Schuster, 2019; West et al., 2007).

It is important to note that not all bioremediation systems correspond to a public goods game (e.g., Smith et al. (1998); Röling et al. (2002)), but here we focus on a subset of these systems, because of their interesting dynamics.

In our model, microbes can adopt one of four strategies: they can be enzyme secretors that pay a cost to contribute to the public good (cooperators) or non-secretors that do not (cheaters). In addition, microbes can be sensitive to the toxins, or can acquire resistance, for example, by activating efflux pumps to expel toxins from within the cell, or thickening the cell wall. In essence, public good secretion can also be seen as a form of resistance to the toxin. In other words, here we consider toxin resistance through private or public means, whereby a cell benefits only itself or also the remaining population, respectively.

The population and evolutionary dynamics are then analyzed using evolutionary game theory (EGT), where a strategy is considered to be evolutionarily stable (ESS) if it is not invaded by mutants with another strategy (Maynard Smith and Price, 1973). EGT typically considers the frequencies of strategies (i.e., frequencies sum to one), for example in the replicator dynamics (Cressman and Tao, 2014). Here, however, since toxin concentration decreases with the absolute number or density of microbes that contribute to degradation (cooperators), our model describes the dynamics of the densities of strategies (as in Hauert et al. (2006, 2008); Gokhale and Hauert (2016)). And since the microbes' death rate depends on toxin concentration in the environment and their resistance level, our model also includes environmental feedback (as in Gong et al. (2018); Tilman et al. (2019); Weitz et al. (2016)), where each strategy affects the environment differently, and the changing environment affects the fitness of each strategy differently. In sum, our model includes population dynamics, evolutionary dynamics, and environmental feedback.

We use this model to derive a protocol for optimal toxin degradation. We first show that cooperators that secrete toxin-degrading enzymes are excluded by cheaters that do not, if they have the same level of resistance to the toxin. However, cooperators can invade a population of cheaters if their level of toxin resistance is different. Since cheaters are unlikely to acquire double mutations leading to cooperators with a different resistance level, maintaining degradation is only possible if we periodically introduce these cooperators back into the chemostat. We then calculate the values of the experimentally controllable parameters (introduction rates of cooperators, chemostat dilution rates and inflowing toxin concentrations) that maximize the cumulative efficiency of detoxification.

2 Model

In our scenario (Fig. 1A), cells can take on one of four strategies depending on whether they produce the enzymes that degrade the toxin (cooperate) or not (cheat), and whether the cells are resistant to the toxin (resistant) or not (sensitive): sensitive cooperator (sCo), sensitive cheater (sCh), resistant cooperator (rCo), and resistant cheater (rCh).

We begin by defining the bacterial population dynamics in our system. The dynamics of the density x of each strategy $i \in \{\text{sCo}, \text{sCh}, \text{rCo}, \text{rCh}\}$ in a chemostat is defined by growth, death and dilution out of the chemostat:

$$\frac{dx_i}{dt} = x_i \left[r_i \left(1 - \sum_j x_j \right) - \delta_i(T) - \alpha \right], \tag{1}$$

where r_i is the intrinsic growth rate of strategy i due to nutrients that are not explicitly defined in the model, $\delta_i(T)$ is the death rate of strategy i given toxin concentration T, and α is the dilution rate. Note that the total densities of the four strategies $\sum_i x_i$ should be lower or equal to one in Eq (1); i.e., the carrying capacity is normalized to be one. In this formulation, the relative fitness of each strategy W_i is a function of toxin concentration:

$$W_i(T) \equiv \frac{r_i}{\delta_i(T) + \alpha}, \tag{2}$$

which is obtained by dividing *per capita* growth rate $dx_i/x_i dt$ by $\left(1 - \sum_j x_j\right)\{\delta_i(T) + \alpha\}$ and adding $1/\left(1 - \sum_j x_j\right)$. At an equilibrium, $W_i(T) = 1/\left(1 - \sum_j x_j\right)$ should be satisfied for any strategy i that exists in the chemostat ($x_i > 0$). In addition, when the relative fitness of strategy i is larger than that of strategy j, strategy i increases faster or decreases slower than strategy j. For simplicity, this basic model assumes that strategies cannot mutate into each other. We extend it to include mutations in Appendix 5.

First, the intrinsic growth rates in this model differ depending on the costs each strategy pays. Cooperators pay a cost, c_d, for producing degrading enzymes, which are regarded as a public good since they reduce environmental toxicity and the death rate of all cells independently of their strategy. In addition, toxin resistance carries a cost, c_r. Such fitness costs, where resistant cells have lower fitness than sensitive ones in the absence of toxins, have been observed in many antibiotic resistant species (Andersson and Levin, 1999; Andersson and Hughes, 2010; Gagneux, 2009). In contrast to the production of the degrading enzymes, however, where all

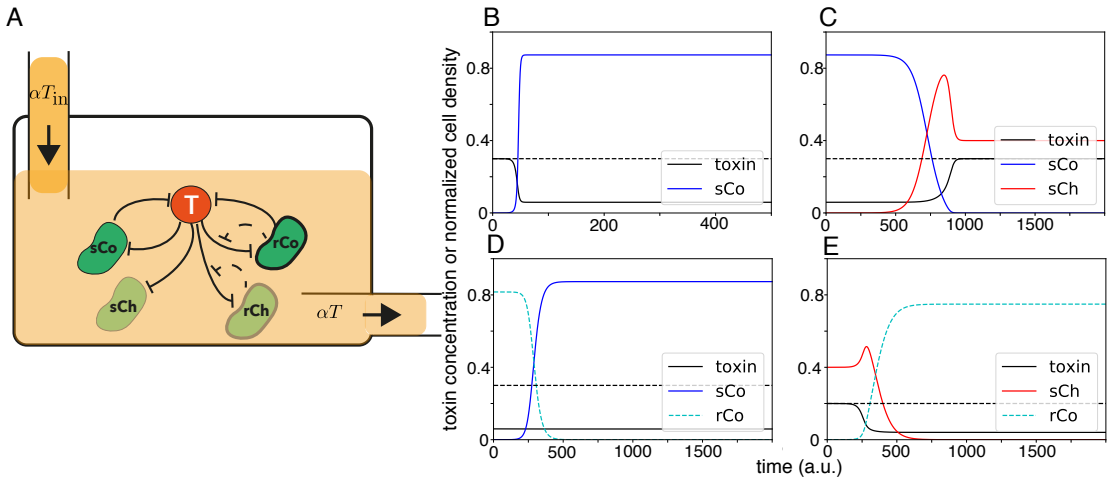

Figure 1: Schematic illustration of the model and examples of the dynamics

(A) In our scenario, a fluid with toxin concentration T_{in} flows into the chemostat while the same amount of fluid with toxin concentration T flows out. The dilution rate of the chemostat is α. Each cell can exhibit one of four strategies: sensitive cooperator (sCo), resistant cooperator (rCo), sensitive cheater (sCh), or resistant cheater (rCh). Cooperators produce enzymes that degrade the toxin, while cheaters do not. The toxin kills cells depending on its concentration, but resistant cells have a lower death rate compared to sensitive cells. Whether the cells are cooperators or cheaters is independent of their resistance level and vice versa. (B-E) Examples of the dynamics in the absence of mutation are shown. In each panel, the black solid line represents the toxin concentration T while the dashed black line is the toxin concentration flowing into the chemostat T_{in}. Detoxification efficiency is proportional to the area between dashed and solid black lines. Other colored lines represent the cell densities of one of the four strategies (solid blue line: sCo, dashed cyan line: rCo, solid red line: sCh). (B) sCo grows and degrades the toxins. (C) sCo is invaded and excluded by sCh. (D) rCo is invaded and excluded by sCo. (E) sCh is invaded and excluded by rCo. Note that the initial conditions in (C-E) are the stable equilibria of the mono-culture of the resident strategies, respectively, while in (B) we begin with a low density of sCo and $T(0) = T_{\text{in}}$. Parameter values are $\alpha = 0.1$, $T_{\text{in}} = 0.2$ (E) or 0.3 (otherwise), $f_{\text{max}} = 0.5$, $K_d = 0.2$, $r = 1$, $c_d = 0.15$, $c_r = 0.2$ (E) or 0.3 (otherwise), $d_{\text{max}} = 1$, $K_s = 0.2$ (E) or 0.3 (otherwise), $K_r = 0.6$, and $n = 1$ (E) or 3 (otherwise).

cells benefit from decreased toxicity, the evolution of resistance can be regarded as an investment into a private good, where only the resistant cells themselves benefit. Then, the intrinsic growth rate r_i of each strategy is defined as follows:

$$r_{\mathrm{sCo}} = r\left(1 - c_d\right) \tag{3a}$$
$$r_{\mathrm{sCh}} = r \tag{3b}$$
$$r_{\mathrm{rCo}} = r\left(1 - c_d - c_r\right) \tag{3c}$$
$$r_{\mathrm{rCh}} = r\left(1 - c_r\right), \tag{3d}$$

where r is the maximum intrinsic growth rate.

Cellular death rate $\delta_i(T)$ increases with toxin concentration T, and is represented by a Hill equation as is common in models of death by antibiotics (Chou et al., 2010; Mougabure-Cueto and Sfara, 2016):

$$\delta_i\left(T; K\right) = d_{\max}\frac{T^n}{T^n + K_i^n}, \tag{4}$$

where $d_{\max}$ is the maximum death rate, K_i is the median-effect concentration of strategy i, and n is the Hill coefficient. Resistance can be modeled either by increasing K or decreasing n (Sampah et al., 2011). For simplicity, we assume that resistant cells have a larger K than sensitive cells: $K_r > K_s$. Note that the toxin concentration T changes over time (the dynamics are defined later).

Due to the dilution in the chemostat, a proportion of cells of each strategy i flows out of the chemostat. The dilution rate into and out of the system is denoted by α.

To describe the population dynamics of each strategy, however, it is necessary to also formulate the dynamics of the toxin concentration because it affects the microbes' death rate, and because the toxin concentration changes over time as cooperators detoxify it. The dynamics of the toxin concentration T in the chemostat are defined by the concentration flowing into and out of the chemostat, and detoxification by cooperators:

$$\frac{dT}{dt} = \alpha T_{\mathrm{in}} - f\left(x_{\mathrm{Co}}\right)T - \alpha T, \tag{5}$$

where T_{in} is the toxin concentration flowing into the chemostat, and $f\left(x_{\mathrm{Co}}\right)$ is the degradation rate which is assumed to follow a Michaelis-Menten function

$$f\left(x_{\mathrm{Co}}\right) = f_{\max}\frac{x_{\mathrm{Co}}}{x_{\mathrm{Co}} + K_d}, \tag{6}$$

where $x_{\mathrm{Co}} = x_{\mathrm{sCo}} + x_{\mathrm{rCo}}$; i.e., the sum of sensitive and resistant cooperators. This function represents half of the maximum degradation rate of the toxin $f_{\max}/2$ when $x_{\mathrm{Co}} = K_d$. All parameters of the model are listed in Table 1.

Table 1: List of parameters

Notation	Range	Description
α	$(0, 1]$	dilution rate of the chemostat
r	$(0, 1]$	maximum intrinsic growth rate of the microbe
c_d	$(0, 1]$	cost of cooperation (production of the degrading enzyme)
c_r	$(0, 1]$	cost of resistance to the toxin
$d_{\max}$	$(0, 1]$	maximum death rate by toxin
K_s	$[0, K_r)$	median-effect toxin concentration of the sensitive cells
K_r	$(K_s, 1]$	median-effect toxin concentration of the resistant cells
n	$(0, \infty]$	Hill coefficient
T_{in}	$(0, 1]$	toxin concentration flowing into the system
$f_{\max}$	$(0, 1]$	maximum degradation rate of the toxin
K_d	$(0, 1]$	median-effect density of the degradation rate
μ_1	$[0, 1]$	mutation rate in the function of detoxification
μ_2	$[0, 1]$	mutation rate in the resistance level

As the goal of this study is to maximize the efficiency of detoxification, we define detoxification efficiency ϕ as the difference between the toxin concentration flowing into and out of the chemostat multiplied by the dilution rate:

$$\phi\left(\alpha, T_{\mathrm{in}}, T\right) = \alpha\left(T_{\mathrm{in}} - T\right). \tag{7}$$

With this definition, ϕ is proportional to the amount of detoxified liquid and is composed of the degree of detoxification and the amount of liquid flowing out of the chemostat. Although this equation gives the efficiency at any time t, we mainly focus on the efficiency at an equilibrium.

3 Results

We first analyze the population dynamics in the case of a mono-culture of cooperators. This is because the analysis of the evolutionary dynamics is meaningless if cooperators cannot persist in mono-culture and because this analysis facilitates the understanding of the evolutionary dynamics, which we shall see later. After finding the stable equilibrium in both the mono- and co-culture scenarios, we shall see how to maximize detoxification efficiency by changing the culture conditions.

3.1 Population and evolutionary dynamics

3.1.1 All strategies can persist in mono-cultures with no mutation

We first analyse the population dynamics of cooperators. Here, it is reasonable to assume that $T(0) = T_{\text{in}}$ because, without cooperators, the concentration of toxins flowing out of the chemostat converges to T_{in}.

When cooperators (either sensitive or resistant) are introduced into the system at a small density, $0 < x_i(0) \ll 1$, they increase and converge to a non-trivial equilibrium where their density is positive (Fig. 1B) if and only if

$$r_i > \delta_i\left(T_{\text{in}}\right) + \alpha \Leftrightarrow W_i\left(T_{\text{in}}\right) > 1, \tag{8}$$

where i is the focal strategy, here $i \in \{\text{sCo}, \text{rCo}\}$ (see Appendix 1 for derivation). This is straightforward because cooperators can only increase at first if inequality (8) is satisfied. However, we also require the system to be free of oscillations in population sizes, otherwise it will be difficult to analyze the stability and the efficiency of detoxification (but see (Weitz et al., 2016)). By solving $dT/dt = 0$ and $dx_i/dt = 0$, one can find a trivial equilibrium $(T, x_i) = \left(T_{\text{in}}, 0\right)$ and one or more non-trivial equilibria where $x_i > 0$. A non-trivial equilibrium should satisfy:

$$T^* = \frac{\alpha T_{\text{in}}}{\alpha + f\left(x_i^*\right)}, \tag{9a}$$

$$x_i^* = 1 - \frac{\delta_i\left(T^*\right) + \alpha}{r_i}. \tag{9b}$$

Due to the non-linearity of the system, it is impossible to calculate this equilibrium point in a closed form. However, one can numerically calculate it using Newton's method.

In the case of a mono-culture of cheaters, the toxin concentration remains at $T = T_{\text{in}}$ regardless of cell density, and their density at a stable equilibrium is positive if inequality (8) holds for the cheaters ($i \in \{\text{sCh}, \text{rCh}\}$), where $T^* = T_{\text{in}}$, and x_i^* is given by Eq (9b). See Appendix 1 for details.

3.1.2 Cheaters can invade a population of cooperators

From now on, we will focus on conditions where the density of each of the four strategies converges to a positive fixed value in mono-culture, which holds when $r_i > \delta_i\left(T_{\text{in}}\right) + \alpha$, where $i \in \{\text{sCo}, \text{sCh}, \text{rCo}, \text{rCh}\}$. Next, we relax the assumption that mutations never occur, and assume that one of two mutations can occur: cooperators mutate into cheaters or vice versa, and sensitive cells become resistant to the toxins or vice versa. For simplicity, however, we still assume that the mutation rates are very small and that the dynamics of each strategy are governed by Eq (1). We then perform a pairwise invasion analysis where one mutant appears in the population of one of the four strategies at the non-trivial equilibrium. Fig. 2A shows the summary of this analysis and Figs. 2B-E represent the main results of the invasion analysis.

First, we analyzed the cases when mutation changes only one trait at a time. Cheater mutants can always invade and exclude a population of cooperators as long as they have the same resistance levels (e.g., sCo and sCh). This applies at any toxin concentration and independently of whether they are both sensitive or both resistant (Fig. 1C). This is because cooperators pay a cost for producing degrading enzymes (cooperators have a smaller intrinsic growth rate than cheaters), while the death rates of cooperators and cheaters caused by the toxin are the same. In other words, the tragedy of commons (Hardin, 1968) occurs in this case.

3.1.3 Toxin concentration determines invasion of sensitive and resistant cells

For mutants that only differ in their resistance level (e.g., sCo and rCo), on the other hand, the toxin concentration determines whether invasion succeeds or not. Intuitively, this is because resistance to the toxin can be costly when the toxin concentration is either very low or very high. Under these conditions, the difference in death rate between sensitive and resistant cells is small, and sensitive cells can invade the population of resistant ones (Fig. 1D). In contrast, resistant cells can invade a population of sensitive cells when the toxin concentration in the chemostat is intermediate. These mutants never stably coexist with the resident strains (Fig. 2, see Appendix 3 for derivation).

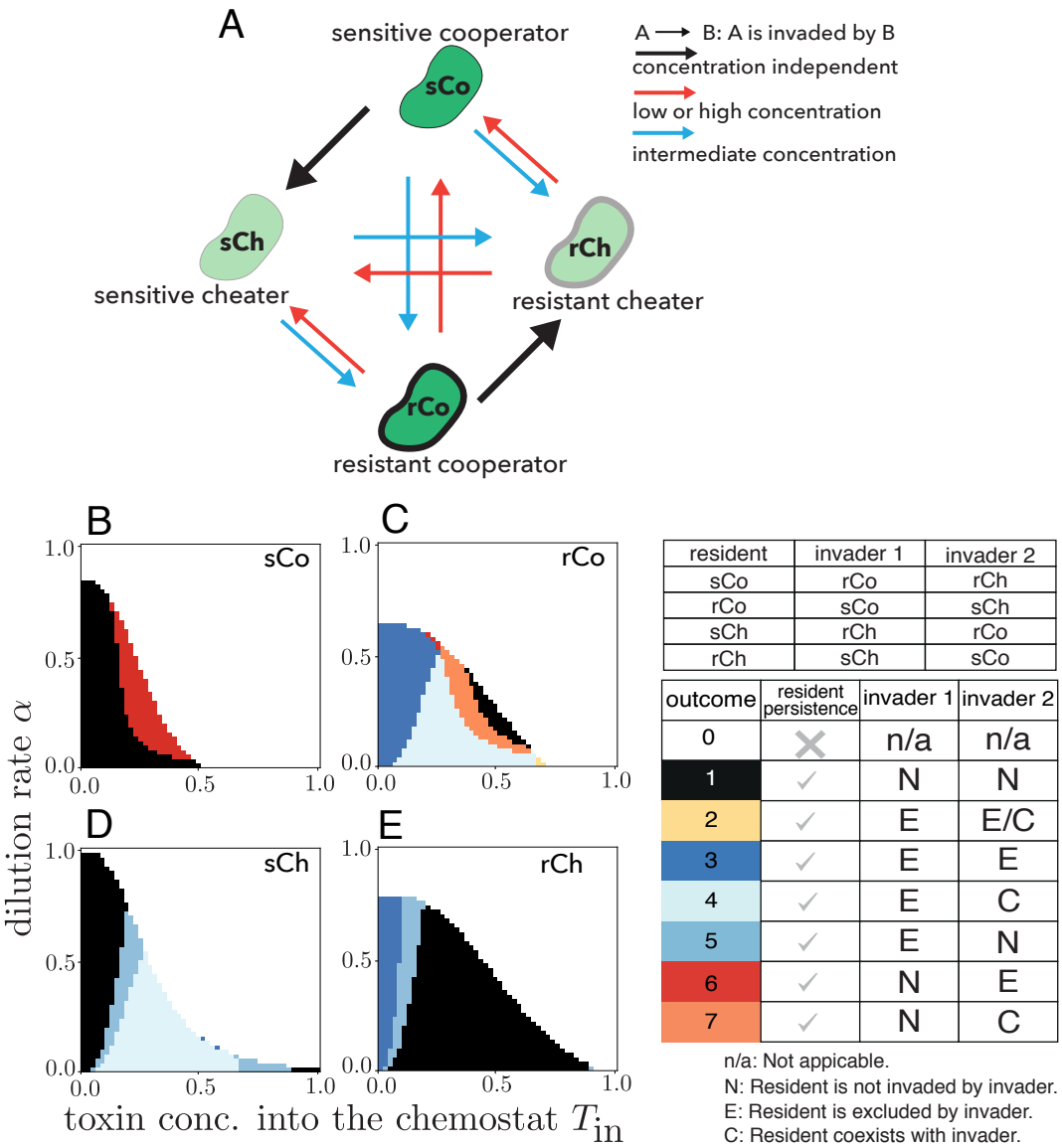

resident	invader 1	invader 2
sCo	rCo	rCh
rCo	sCo	sCh
sCh	rCh	rCo
rCh	sCh	sCo

outcome	resident persistence	invader 1	invader 2
0	✗	n/a	n/a
1	✓	N	N
2	✓	E	E/C
3	✓	E	E
4	✓	E	C
5	✓	E	N
6	✓	N	E
7	✓	N	C

Figure 2: Summary of the pairwise invasion analysis as short-term evolutionary dynamics

(A) Diagram of pairwise invasion analysis. A → B represents that A is invaded by B, and the color of each arrow shows the condition for successful invasion. Black arrows represent successful invasion regardless of the toxin concentration, while red and sky blue arrows represent toxin-concentration-dependent invasion. Red arrows show that invasion succeeds when the toxin concentration is low or high. Sky blue arrows indicate that the invasion succeeds when the toxin concentrations are at an intermediate level. (B-E) The state space of invasion analysis when the resident strategy is sCo (B), rCo (C), sCh (D), or rCh (E). As cheaters always exclude cooperators when they have the same resistance level, we analyzed whether the resident strategies are invaded by the other two types of invaders. Here, an invader that does not differ in cooperativity is called invader 1 and the other type invader 2 (e.g., if the resident is sCo, invader 1 is rCo and invader 2 is rCh). Colors represent the results of the invasion analysis given culture conditions α and T_{in}. Color in each panel classifies the results of invasion analysis, and the results of invasion analysis are shown in the table beside the panels C and E. Note that the white (class 0) area represents where the resident strategy is not maintained as Eq (8) is not satisfied before the invasion. Parameter values in (B-E) are $f_{\max} = 0.5$, $K_d = 0.2$, $r = 1$, $c_d = 0.15$, $c_r = 0.2$, $d_{\max} = 1$, $K_s = 0.3$, $K_r = 0.6$, and $n = 3$. Note that panels (B-E) are examples of the state space given the parameter values; different parameter values will show different invasion landscapes, as summarized in panel (A).

3.1.4 Cooperators can invade cheaters of different resistance levels

Next, we consider cases where cooperators and cheaters differ in their ability to resist the toxin, and either strategy is invading the other. We find that rCo can invade a population of sCh at specific toxin concentrations, while at other concentrations, it is sCo that can invade rCh (blue, gray blue, or cyan area in Figs. 2D and E). This follows the same logic as for the invasion of resistant mutants into a sensitive population described above: when the toxin concentration is intermediate, rCo have a much lower death rate than sCh, and the benefit of resistance exceeds the sum of the cost of cooperation c_d and resistance c_r. If, on the other hand, the toxin concentration is either too low or too high, resistance to the toxin does not provide enough of an advantage to overcome its cost, leading to the invasion of sCo into a population of rCh. In sum, whether rCo invades sCh or sCo invades rCh depends on toxin concentrations. The range of toxin concentrations where invasion is successful is analytically calculated in Appendix 2.

3.1.5 Cooperators and cheaters can stably co-exist in the short-term

Given that these cooperators and cheaters with different resistance levels can invade each other, we next ask whether one strategy excludes the other entirely or whether they will coexist. This is unclear because, as cooperators increase, toxin concentration decreases, which changes the fitness landscape. In other words, increasing cooperator density can decrease the fitness difference between cooperators and cheaters. If the strategies do coexist, we next analyze the evolutionary dynamics to determine whether the system converges to a fixed point or shows oscillations as reported in (Gong et al., 2018; Tilman et al., 2019; Weitz et al., 2016).

For simplicity, let us denote i as the cooperators and j as the cheaters. In the evolutionary dynamics after cooperators i invade the population of cheaters j, two equilibria are possible. In the first, cheaters j are excluded $(T, x_i, x_j) = (T_i^*, x_i^*, 0)$ and T_i^* and x_i^* are equivalent to the stable equilibrium of the mono-culture of cooperators i. The second equilibrium is where cooperators i and cheaters j coexist; i.e., $(T, x_i, x_j) = \left(T_{ij}^\dagger, x_i^\dagger, x_j^\dagger\right)$. At this equilibrium, the relative fitness of cooperators i and cheaters j are equal at toxin concentration $T_{ij}^\dagger$. The equilibrium and the conditions under which it is stable are analytically derived in Appendix 3.

In Appendix 4, we further show that if cooperators and cheaters of different resistance levels (e.g. rCo and sCh) coexist, they can be invaded by cheaters with different resistance (e.g. rCh), which excludes the other two strategies. In other words, cooperators are never evolutionarily stable because they can be invaded and excluded by cheaters of the same resistance level.

3.1.6 Long-term evolutionary dynamics predict that cooperators are unlikely to be maintained

Based on the results of the invasion analysis of mutants in the short-term (Fig. 2A), the long-term evolutionary dynamics can be represented by the state transition diagram in Fig. 3. The probability of state transitions is given by the mutation rates (μ_1: change of cooperators to cheaters or vice versa, μ_2: change in the level of resistance), while the short-term evolutionary dynamics are governed by Eq (1). For example, sCh will appear in the population of sCo with probability $\mu_1 (1 - \mu_2)$ and exclude it. Then, rCh can appear in the population of sCh with probability $(1 - \mu_1)\, \mu_2$, but may invade or not, depending on the toxin concentration.

Although in principle cooperators can invade a population of cheaters that differ in the level of resistance (e.g., rCo can invade sCh), (i) invasion success depends on α and T_{in}, and (ii) double mutations are expected to be rare ($\mu_1\mu_2$ close to 0). Accordingly, it is very difficult to maintain cooperators in the chemostat due to natural selection. In other words, to maintain costly microbial detoxification, it is necessary to manually introduce cooperators (Fig. 3 blue arrows) and to change α and T_{in} to favor their survival. In the following section, we show how to control the values of α and T_{in} to maximize the efficiency of detoxification. It should be noted that the evolutionary dynamics governed by Eq (2) lead to the same conclusion when small mutation rates are introduced into Eq (2) (see Appendix 5).

3.2 Optimizing detoxification efficiency

3.2.1 Culture conditions can be controlled to optimize detoxification efficiency

We now analyze how to maximize the efficiency of detoxification ϕ by changing the culture conditions through two parameters: the dilution rate α and the toxin concentration flowing into the chemostat T_{in}. In the next section, we focus on the third parameter that can help maximize detoxification: the manual introduction rates of each cooperator (m_1 for sCo, and m_2 for rCo).

To maximize the objective function in Eq (7), we consider three equilibrium states with different toxin concentrations flowing out of the chemostat: (i) $T = T_{\text{in}}$ when only cheaters are present, (ii) $T = T_{ij}^\dagger$ when cooperators i coexist with cheaters j, which have different resistant levels, and (iii) $T = T_i^*$ when only one type of cooperators i is present. If only cheaters, who cannot degrade the toxin, are present, the objective function remains zero ($T = T_{\text{in}}$) regardless of the values of α and T_{in}. When cooperators coexist with cheaters of different

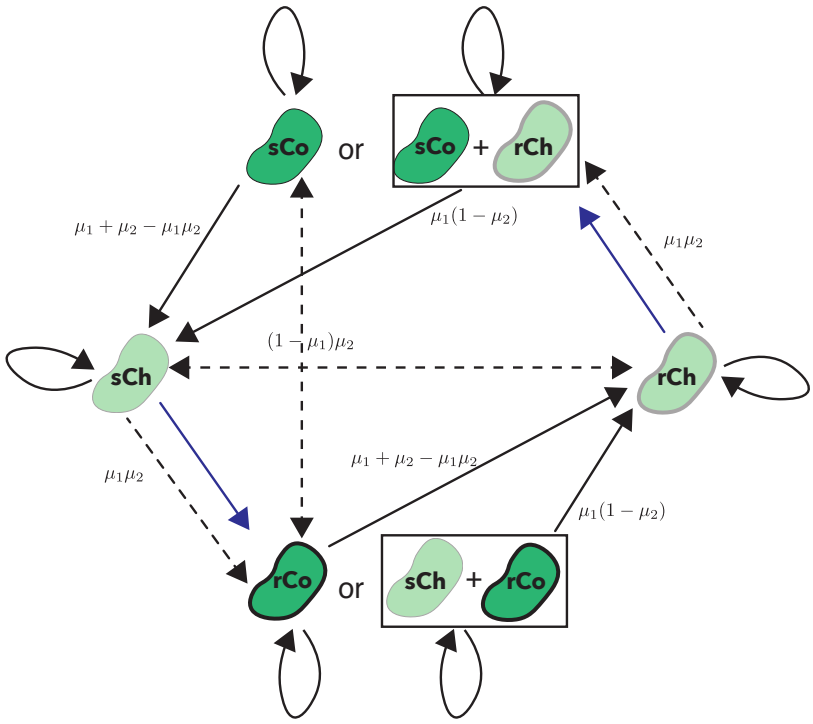

Figure 3: Schematic illustration of the state transitions for long-term evolutionary dynamics

Summary of the population state transitions. Black arrows represent state transitions caused by natural selection (solid arrows: toxin concentration independent, and dashed ones: toxin concentration dependent), while blue arrows represent the manual introduction of cooperators. It should be noted that the vertical transition (from sCo to rCo and vice versa) does not occur if cooperators coexist with cheaters. Each value along the arrows represents the state transition probability.

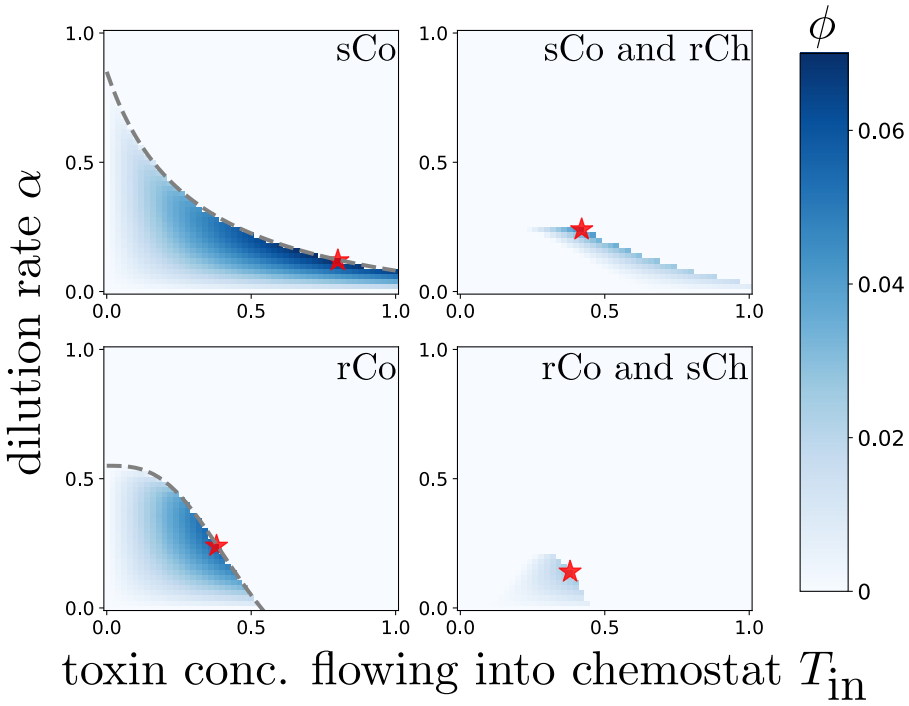

Figure 4: Optimal detoxification at each equilibrium

The efficiency of detoxification at an equilibrium state $\phi\left(\alpha, T_{\text{in}}, T\right)$ given α and T_{in} is represented by color in each panel (top right: only sCo, top left: coexistence of sCo with rCh, bottom left: only rCo, and bottom right: coexistence of rCo with sCh). The red stars represent the maximum efficiency of detoxification in each. In the areas above the dashed gray lines in each two left panels, the cooperator cannot persist in mono-culture (inequality 8). Parameter values are $f_{\max} = 0.5$, $K_d = 0.2$, $r = 1$, $c_d = 0.15$, $c_r = 0.3$, $d_{\max} = 1$, $K_s = 0.3$, $K_r = 0.5$, and $n = 1$ (top row: sCo) or $n = 3$ (bottom row: rCo). We used different values of n in the top and bottom rows to allow cooperators to coexist with cheaters with a different level of resistance.

resistance levels, one can analytically find the equilibria and their corresponding detoxification efficiency for each culture condition (values of α and T_{in}). We can then find the optimal culture conditions that maximize this efficiency, although the equilibrium can be unstable for some parameter values (Fig. 4 top and bottom right). If only cooperators are present, it is difficult to analytically find the optimal efficiency because one cannot calculate T_i^* in a closed form. Instead, we numerically computed the equilibria for different culture conditions $\left(\alpha, T_{\text{in}}\right)$ and the corresponding detoxification efficiency ϕ, allowing us to find the global maximum of ϕ (Fig. 4 top and bottom left).

Intuitively, the maximum efficiency is larger in a mono-culture of cooperators than in a co-culture of cooperators and cheaters of different levels of resistance (see Appendix 6 for more detail). If cheaters can be excluded from the population by changing α and T_{in}, the optimal strategy for cultivation is (i) to exclude the cheaters by adjusting the culture conditions, and then (ii) to change the culture conditions to maximize the productivity of a mono-culture of cooperators.

3.2.2 Cooperators can be introduced at rates that optimize detoxification efficiency

In section 3.1.2, we found that cooperators can invade a population of cheaters if their level of resistance is different. However, cooperators that differ in their resistance from the resident cheaters are unlikely to appear by mutation (Fig. 3). Therefore, it would be more efficient to manually introduce cooperators into the population, and to change α and T_{in} to allow them to invade successfully and to exclude the cheaters. Assuming that we cannot observe the state of the population (i.e., the prevalence of each strategy) at any given point in time, the problem is how often to introduce sensitive or resistant cooperators (m_1 and m_2, respectively) to maximize detoxification efficiency over time. If cooperator introduction rates are too small, cheaters will dominate the population, leading to a detoxification efficiency of zero (Eq 7). If they are too large, we will introduce cooperators unnecessarily (e.g., introducing sCo into a mono-culture of sCo) or introduce cooperators that cannot invade (e.g., introducing sCo into a mono-culture of sCh). Such unfavorable introductions can be

costly because they can require a higher in-flowing toxin concentration T_{in}, and result in reduced detoxification efficiency for some time.

To optimize cooperator introduction rates, we redefine the time scale from continuous to discrete time steps. We then consider population state transitions as a Markov chain. Let us denote the state distribution vector $\boldsymbol{\pi}(s) = (\pi_i(s))$ where π_i is the probability that the state of the population is i at time step s ($\sum_i \pi_i(s) = 1$ for $s = 0, 1, \ldots, \infty$), and the transition matrix $P(\boldsymbol{m}; \boldsymbol{\mu})$, where $\boldsymbol{m} = (m_1, m_2)$ and $\boldsymbol{\mu} = (\mu_1, \mu_2)$. Then, the probability distribution at time step $s+1$ is derived as follows:

$$\boldsymbol{\pi}(s+1, \boldsymbol{m}; \boldsymbol{\mu}) = \boldsymbol{\pi}(s, \boldsymbol{m}; \boldsymbol{\mu}) P(\boldsymbol{m}; \boldsymbol{\mu}). \tag{10}$$

Now, let us denote the expected cumulative efficiency of detoxification from the beginning of the cultivation to time step s as $\Phi(s, \boldsymbol{m}; \boldsymbol{\mu})$. Then, $\Phi(s+1, \boldsymbol{m}; \boldsymbol{\mu})$ is recursively represented as follows:

$$\Phi(s+1, \boldsymbol{m}; \boldsymbol{\mu}) = \Phi(s, \boldsymbol{m}; \boldsymbol{\mu}) + \sum_i \phi_i \pi_i(s+1, \boldsymbol{m}; \boldsymbol{\mu}), \tag{11}$$

where ϕ_i is the efficiency of detoxification at a given time step when the state of the population is i. The optimization problem is to find the value of $\boldsymbol{m}$ which maximizes $\Phi(s, \boldsymbol{m}; \boldsymbol{\mu})$ given a time step s. From Eq (11), this problem can be solved using Dynamic Programming (DP).

Notice, however, that the Markov chain shown is ergordic (i.e., aperiodic and positive recurrent) when both sensitive and resistant cooperators can exclude cheaters that differ in their resistance level (see Appendix 7 for a case where cooperators cannot exclude cheaters). Then, the probability distribution of the population states converges to a unique stationary distribution $\boldsymbol{\pi}^*$ in the limit of $s \to \infty$, regardless of the initial distribution $\boldsymbol{\pi}(0)$. This stationary distribution is analytically derived as follows:

$$\boldsymbol{\pi}^*(\boldsymbol{m}; \boldsymbol{\mu}) = \boldsymbol{\pi}^*(\boldsymbol{m}; \boldsymbol{\mu}) P(\boldsymbol{m}; \boldsymbol{\mu}). \tag{12}$$

When the state distribution $\boldsymbol{\pi}$ converges to the stationary distribution, the second term of Eq (11) is independent of s. In other words, for large s, the optimization problem given by Eq (11) is approximately simplified to:

$$\hat{\Phi}(\boldsymbol{m}; \boldsymbol{\mu}) \equiv \sum_i \phi_i \pi_i^*(\boldsymbol{m}; \boldsymbol{\mu}). \tag{13}$$

For large s, therefore, the optimal $\boldsymbol{m}$ is obtained that maximizes $\hat{\Phi}$. Finding this optimum has a lower computational complexity than DP, making it easier to solve than Eq (11).

3.2.3 An example of optimizing detoxification efficiency

Let us now imagine that we have set up the experimental system described, and would like to compute the optimal introduction rates. We first need to define the Markov chain that we will use to make predictions, and second, we need to experimentally measure the parameters of our chemostat, in particular the degradation efficiency ϕ_i at each of the different states i of the Markov chain.

To establish the Markov chain, we begin with a few assumptions for simplicity: (i) that mutations and the manual introduction of cooperators can occur only in a mono-culture of one of the four strategies and never at the same time (i.e., at a given point in time, at most two strategies can exist in the population), that (ii) sCo and rCo can mutually exclude each other if we change (α, T_{in}) so that each of them can invade the cheaters that differ in the level of resistance, that (iii) sCo and rCo can exclude rCh and sCh, respectively, at certain (α, T_{in}) and (iv) that $\mu_2 = 0$, such that cooperators can only invade a population of cheaters that differ in the level of resistance by manual introduction. We relax these assumptions in Appendix 7. Under these assumptions, the Markov chain consists of 14 states: four mono-culture situations, six transient situations where two strategies coexist, and four situations where the introduction of cooperators is unfavorable (see Fig. A.9 for the diagram). A simplified schematic of this model is shown in the left panel of Fig. 5.

In this case, the relationship between m_1, m_2 and the stationary distribution $\boldsymbol{\pi}$ can be analytically derived (see Appendix 7). By experimentally measuring $\boldsymbol{\phi} = (\phi_i)$ for each state i and mutation rates $\boldsymbol{\mu}$, we can calculate the probability distribution $\boldsymbol{\pi} = (\pi_i)$ then find the introduction rates m_1, m_2 that will maximize detoxification efficiency Φ and $\hat{\Phi}$ according to Eqs (11) and (13). The two solid lines in the right panel of Fig. 5 represent m_1 and m_2, respectively, which maximize $\Phi(s)$ when the simulation finishes at time step s given some fictitious yet reasonable values of $\boldsymbol{\mu}$ and $\boldsymbol{\phi}$. Here, the initial state of the population is assumed to be a mono-culture of sCo. At first, the optimal values of m_1 and m_2 are zero, because the state of the population at each time step is the most likely to be a mono-culture of sCo, and therefore the introduction of the cooperators is more likely to be a cost. However, as time passes, mutations will arise, and the population is more likely to transition to a state of sCh mono-culture; then, the optimal values of m_1 and m_2 increase. At about 1,000 time steps, the optimal values of m_1 and m_2 converge to the values which maximize detoxification efficiency at the steady state Eq (13).

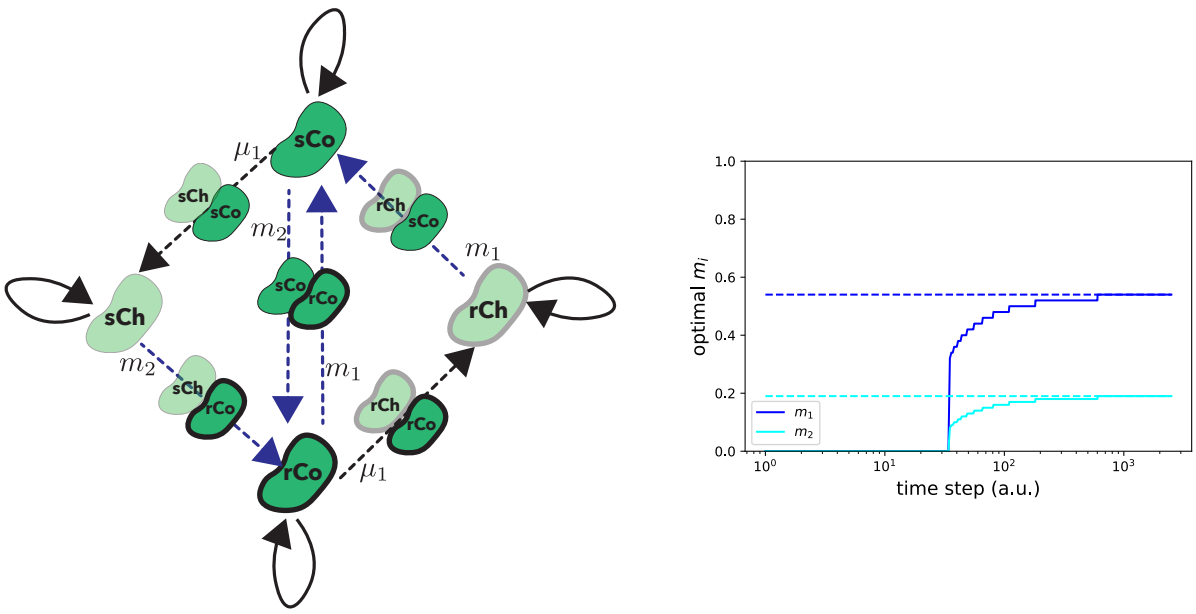

Figure 5: Optimization problem assuming that resistance mutations do not occur

Left: A simplified schematic illustration of the state transition diagram when $\mu_2 = 0$ and cooperators can exclude cheaters of different resistance levels. A $\rightarrow$ B represents a transition from state A to state B. Blue arrows represent transitions that occur through the introduction of cooperators. Dashed arrows suggest the transient states where two strategies coexist. The full diagram containing 14 states is shown in Fig. A.9. Right: The optimal values of m_1 (blue) and m_2 (cyan) which maximize the efficiency defined by Eq (11) is calculated using dynamic programming. The two dashed lines represent the values of m_1 and m_2 which maximize Eq (13). The initial state of the population is a mono-culture of sCo. Around 1,000 time steps, the optimal values of m_1 and m_2 for Eq (11) converge to the values which maximize Eq (13). In practice, the detoxification efficiency at each of the 14 states of the model as well the mutation rates would be experimentally measured and plugged into the model to calculate the values of m_1 and m_2 that would maximize cumulative efficiency. The plot above was generated using the following fictitious values, as an illustration: $\mu_1 = 0.01$, $\mu_2 = 0$, $\boldsymbol{\phi} = \{0.4, 0.2, 0, 0.15, 0.3, 0.15, 0, 0.2, 0.35, 0.35, 0.3, 0, 0.2, 0\}$. See Appendix 7 for more detail.

When $\mu_2 > 0$, the number of states increases and the state transition diagram becomes more complex. If the Markov chains are still ergodic, however, it is possible to find the stationary distribution $\boldsymbol{\pi}^*$ and the optimal values of m_1 and m_2 that maximize Eq (13). If resistant (and/or sensitive) cooperators cannot exclude cheaters with a different level of the resistance, the Markov chain is not ergodic because the mono-culture of cooperators is a transient state. Even in such a case, however, it is possible to find the optimal (m_1, m_2) for the expected cumulative productivity with large s. See Appendix 7 for more detail.

4 Discussion

In this study, we have shown how to control the evolutionary dynamics of a microbial population growing in a chemostat in order to optimize the bioremediation of a toxic liquid. In our model, degrading the toxic compound is costly to the microbes. A cooperative strategy of degrading the compound is therefore not evolutionarily stable because it can be invaded by cheaters that do not degrade. We show, however, that it is possible for cooperators to invade a population of cheaters, but only if they differ in their level of resistance and only at certain toxin concentrations. The co-occurrence of two strains that differ both in their degradation ability as well as their resistance level is unlikely to arise by mutation, especially if we assume that mutations are rare. To maintain the degradation of toxins, therefore, it is necessary to periodically introduce cooperators into the chemostat while changing the dilution rate and toxin concentration flowing into it to guarantee invasion success.

Optimal values for these parameters (cooperator introduction rates, dilution rate, and in-flowing toxin concentration) that maximize the detoxification efficiency of the system can be calculated using our model. As input, the model requires experimental measurements of growth and death rates of the chosen microbe and its mutants (i.e., intrinsic growth rate of each strategy r_i, maximum death rate $d_{\max}$, Hill coefficient n, median-effect toxin concentrations K_s, K_r, and degradation efficiencies ϕ of cooperators).

Our model and its results can also apply to problems other than bioremediation that involve survival in toxic

environments. In essence, we are studying the evolutionary dynamics of public resistance, which is cooperative, and private resistance, which is not. Consider, analogously, two types of antibiotic resistance mechanisms: public mechanisms are costly and benefit the producing cell as well as its neighbors such as extracellular enzyme secretion, and private resistance mechanisms only benefit the producing cells, such as efflux pumps. The evolutionary dynamics in a scenario whereby cells can switch between these different resistance mechanisms and being sensitive to the antibiotic correspond to Fig. 2A. In this case, however, an objective function would aim to maximize the densities of the least rather than the most resistant strains. Another interesting aspect is that the benefits of resistance depend on toxin concentration in the chemostat, which is affected by the density of cooperators and the toxin concentration flowing into the chemostat. In other words, the public goods game affects the benefit of the private goods. This is why cooperators can invade a population of cheaters when they differ in their resistance level (Fig. 2A).

Of course, our model relies on a number of assumptions and focuses only on a subset of possible bioremediation systems. First, we only consider toxin degradation by extracellular enzyme secretion, while toxins can also be degraded inside cells (O'Brien and Brockhurst, 2015). For intra-cellular degradation, a different functional form of detoxification $f(x_{\mathrm{Co}})$ would be necessary, but we expect similar results as long as this function increases monotonically with the density of cooperators. Indeed, the invasion analysis is independent of the form of $f(x_{\mathrm{Co}})$. Similarly, we assume that toxins kill the microbes and that their degradation does not contribute to growth. In reality, many compounds that are undesirable for humans are instead used as substrates by microbes (Atashgahi et al., 2018). This latter case is simpler than the one we consider here, since detoxification is no longer cooperative and there is no risk of cheaters arising and collapsing the system. Finally, detoxification may carry a negligible cost, for example if it the toxic compound is neutralized by a change in pH, which occurs naturally due to a microbe's metabolism.

Another issue is how to define detoxification efficiency ϕ. Rather than Eq (7) one could, for example, define ϕ as the time needed for the toxins to decrease to a negligible concentration. This would change the optimal culture conditions α and T_{in}, but not the optimal introduction rates of cooperators $\boldsymbol{m}$, which are independent of the formulation of ϕ. Our model also fixes some parameters, such as the Hill coefficient n, which can evolve in reality (Sampah et al., 2011). Similarly, the cost of resistance c_r can decrease over time due to compensatory evolution (Andersson and Hughes, 2010; Millan et al., 2014). Allowing these parameters to evolve would make it more difficult for sCo to invade rCh because the relative fitness of rCh will increase.

We also assume that our system is well-mixed and that there are no spatial gradients within the chemostat. Spatial structure, for example, whereby detoxifying enzymes diffuse slowly through the chemostat and have a patchy distribution can favor the coexistence of cooperators and cheaters (Allison, 2005). Previous empirical bioremediation studies have reported such coexistence (Ellis et al., 2007; O'Brien et al., 2014). Theoretically, this may be due to a difference of resistance levels between cooperators and cheaters as we show here, but a simpler explanation would be the presence of spatial gradients. Relaxing the assumption of a perfectly well-mixed chemostat would make the persistence of cooperators easier.

Finally, there may be other ways of periodically introducing cooperators. Experimentally, our constant introduction rates represent a situation where stock strains of cooperators would be inoculated into the chemostat. If instead, multiple chemostats are running in parallel, another way of introducing cooperators would be to exchange certain amounts of fluids between chemostats. Ecologically, this would correspond to migration rates among patches, and the optimal migration rates would depend on the probability distribution of the different strategies in each chemostat. Comparing the optimal introduction rates and the cumulative efficiency of detoxification between the model presented here and a multi-chemostat system is left for future work.

In summary, we have used evolutionary game theory to develop a protocol for the control and optimization of a bioremediation system by microbes, and guard it against collapse through the emergence of cheaters. The predictions of our model are ready to be tested in the laboratory, and ultimately, at an industrial scale.

5 Acknowledgements

SS is funded by the Nakajima foundation and the University of Lausanne and SM by European Research Council Starting Grant 715097.

References

Tetsuya Akita and Masashi Kamo. Theoretical lessons for increasing algal biofuel: Evolution of oil accumulation to avert carbon starvation in microalgae. *Journal of Theoretical Biology*, 380:183–191, 2015. ISSN 10958541. doi: 10.1016/j.jtbi.2015.05.027. URL http://dx.doi.org/10.1016/j.jtbi.2015.05.027.

Steven D. Allison. Cheaters, diffusion and nutrients constrain decomposition by microbial enzymes in spatially

structured environments. *Ecology Letters*, 8(6):626–635, 2005. ISSN 1461023X. doi: 10.1111/j.1461-0248.2005.00756.x.

Dan I. Andersson and Diarmaid Hughes. Antibiotic resistance and its cost: is it possible to reverse resistance? *Nature Reviews Microbiology*, 8(4):260–271, 4 2010. ISSN 1740-1526. doi: 10.1038/nrmicro2319. URL http://dx.doi.org/10.1038/nrmicro2319http://www.nature.com/articles/nrmicro2319.

Dan I. Andersson and Bruce R. Levin. The biological cost of antibiotic resistance. *Current Opinion in Microbiology*, 2(5):489–493, 10 1999. ISSN 13695274. doi: 10.1016/S1369-5274(99)00005-3. URL http://linkinghub.elsevier.com/retrieve/pii/S1369527499000053.

Dominik Antoni, Vladimir V. Zverlov, and Wolfgang H. Schwarz. Biofuels from microbes. *Applied Microbiology and Biotechnology*, 77(1):23–35, 10 2007. ISSN 0175-7598. doi: 10.1007/s00253-007-1163-x. URL http://link.springer.com/10.1007/s00253-007-1163-x.

Siavash Atashgahi, Irene Sánchez-Andrea, Hermann J. Heipieper, Jan R. van der Meer, Alfons J. M. Stams, and Hauke Smidt. Prospects for harnessing biocide resistance for bioremediation and detoxification. *Science*, 360 (6390):743–746, 5 2018. ISSN 0036-8075. doi: 10.1126/science.aar3778. URL http://dx.doi.org/10.1016/B978-1-4377-2242-0/00034-1http://www.sciencemag.org/lookup/doi/10.1126/science.aar3778.

Jean-Claude Bertrand, Pierre Doumenq, Rémy Guyoneaud, Benoit Marrot, Fabrice Martin-Laurent, Robert Matheron, Philippe Moulin, and Guy Soulas. Applied Microbial Ecology and Bioremediation. In Jean-claude Bertrand, Pierre Caumette, Philippe Lebaron, Robert Matheron, Philippe Normand, and Telesphore Sime-Ngando, editors, *Environmental Microbiology: Fundamentals and Applications*, chapter 16, pages 659–753. Springer Netherlands, Dordrecht, 1st edition, 2015. ISBN 9789401791182. doi: 10.1007/978-94-017-9118-2.

Mark Broom, Karan Pattni, and Jan Rychtář. Generalized Social Dilemmas: The Evolution of Cooperation in Populations with Variable Group Size. *Bulletin of Mathematical Biology*, pages 1–32, 12 2018. ISSN 0092-8240. doi: 10.1007/s11538-018-00545-1. URL http://link.springer.com/10.1007/s11538-018-00545-1.

James J. Bull and Jeffrey E. Barrick. Arresting Evolution. *Trends in Genetics*, 33(12):910–920, 2017. ISSN 13624555. doi: 10.1016/j.tig.2017.09.008. URL http://dx.doi.org/10.1016/j.tig.2017.09.008.

Bradley J. Cardinale, J. Emmett Duffy, Andrew Gonzalez, David U. Hooper, Charles Perrings, Patrick Venail, Anita Narwani, Georgina M. Mace, David Tilman, David A.Wardle, Ann P. Kinzig, Gretchen C. Daily, Michel Loreau, James B. Grace, Anne Larigauderie, Diane S. Srivastava, and Shahid Naeem. Biodiversity loss and its impact on humanity. *Nature*, 489(7415):326–326, 2012. ISSN 0028-0836. doi: 10.1038/nature11373. URL http://www.nature.com/doifinder/10.1038/nature11373.

Yuancai Chen, Che Jen Lin, Gavin Jones, Shiyu Fu, and Huaiyu Zhan. Enhancing biodegradation of wastewater by microbial consortia with fractional factorial design. *Journal of Hazardous Materials*, 171(1-3):948–953, 2009. ISSN 03043894. doi: 10.1016/j.jhazmat.2009.06.100.

Ting-chao Chou, Elena Kurin, Pavel Mučaji, Milan Nagy, Maria Hidalgo, Concepción Sánchez-Moreno, Sonia de Pascual-Teresa, P. Iacopini, M. Baldi, P. Storchi, L. Sebastiani, Ting-chao Chou, Shanshan Wang, Dongmei Wang, and Zehua Liu. Flavonoid–flavonoid interaction and its effect on their antioxidant activity. *Journal of Food Composition and Analysis*, 67(3):621–681, 2010. ISSN 03088146. doi: 10.1124/pr.58.3.10. URL http://linkinghub.elsevier.com/retrieve/pii/S0926669015000278%5Cnhttp://linkinghub.elsevier.com/retrieve/pii/S0889157508000653%5Cnhttp://linkinghub.elsevier.com/retrieve/pii/S0308814610000464%5Cnhttp://www.mdpi.com/1420-3049/17/12/14336/%5Cnhttp://www.sco.

R. Cressman and Y. Tao. The replicator equation and other game dynamics. *Proceedings of the National Academy of Sciences*, 111(Supplement_3):10810–10817, 2014. ISSN 0027-8424. doi: 10.1073/pnas.1400823111. URL http://www.pnas.org/cgi/doi/10.1073/pnas.1400823111.

Ruchita Dixit, Wasiullah, Deepti Malaviya, Kuppusamy Pandiyan, Udai Singh, Asha Sahu, Renu Shukla, Bhanu Singh, Jai Rai, Pawan Sharma, Harshad Lade, and Diby Paul. Bioremediation of Heavy Metals from Soil and Aquatic Environment: An Overview of Principles and Criteria of Fundamental Processes. *Sustainability*, 7(2):2189–2212, 2 2015. ISSN 2071-1050. doi: 10.3390/su7022189. URL http://www.mdpi.com/2071-1050/7/2/2189.

Richard J. Ellis, Andrew K. Lilley, Samantha J. Lacey, David Murrell, and H. Charles J. Godfray. Frequency-dependent advantages of plasmid carriage by Pseudomonas in homogeneous and spatially structured environments. *ISME Journal*, 1(1):92–95, 2007. ISSN 17517362. doi: 10.1038/ismej.2007.11.

S. Gagneux. Fitness cost of drug resistance in Mycobacterium tuberculosis. *Clinical Microbiology and Infection*, 15(SUPPL. 1):66–68, 2009. ISSN 14690691. doi: 10.1111/j.1469-0691.2008.02685.x. URL http://dx.doi.org/10.1111/j.1469-0691.2008.02685.x.

Chaitanya S. Gokhale and Christoph Hauert. Eco-evolutionary dynamics of social dilemmas. *Theoretical Population Biology*, 111:28–42, 2016. ISSN 10960325. doi: 10.1016/j.tpb.2016.05.005. URL http://dx.doi.org/10.1016/j.tpb.2016.05.005.

Lulu Gong, Jian Gao, and Ming Cao. Evolutionary Game Dynamics for Two Interacting Populations under Environmental Feedback. *arxXiv*, 6 2018. URL http://arxiv.org/abs/1806.03194.

Garrett Hardin. The Tradegy of the Commons. *Science*, 162(June):1243–1248, 1968. ISSN 0036-8075. doi: 10.1126/science.162.3859.1243.

Christoph Hauert, Miranda Holmes, and Michael Doebeli. Evolutionary games and population dynamics: maintenance of cooperation in public goods games. *Proceedings of the Royal Society B: Biological Sciences*, 273(1600):2565–2571, 10 2006. ISSN 0962-8452. doi: 10.1098/rspb.2006.3600. URL http://rspb.royalsocietypublishing.org/cgi/doi/10.1098/rspb.2006.3717.

Christoph Hauert, Joe Yuichiro Wakano, and Michael Doebeli. Ecological public goods games: Cooperation and bifurcation. *Theoretical Population Biology*, 73(2):257–263, 2008. ISSN 00405809. doi: 10.1016/j.tpb.2007.11.007.

Sabine Hummert, Katrin Bohl, David Basanta, Andreas Deutsch, Sarah Werner, Günter Theißen, Anja Schroeter, and Stefan Schuster. Evolutionary game theory: cells as players. *Mol. BioSyst.*, 10(12):3044–3065, 2014. ISSN 1742-206X. doi: 10.1039/C3MB70602H. URL http://xlink.rsc.org/?DOI=C3MB70602H.

Chang-ho Kang, Yoon-jung Kwon, and Jae-seong So. Bioremediation of heavy metals by using bacterial mixtures. *Ecological Engineering*, 89:64–69, 4 2016. ISSN 09258574. doi: 10.1016/j.ecoleng.2016.01.023. URL http://dx.doi.org/10.1016/j.ecoleng.2016.01.023https://linkinghub.elsevier.com/retrieve/pii/S0925857416300234.

P. K. R. Kumar, H.E Maschke, K. Friehs, and K. Schügerl. Strategies for Improving Plasmid Stability in Bioreactors. *Trends in Biotechnology*, 9(8):279–284, 1991.

David J. Lea-Smith and Christopher J. Howe. The Use of Cyanobacteria for Biofuel Production. In John Love and John A. Bryant, editors, *Biofuels and Bioenergy*, chapter 9, pages 143–155. John Wiley & Sons, Ltd, Chichester, UK, 1 edition, 3 2017. ISBN 9781118350560. doi: 10.1002/9781118350553.ch9. URL http://doi.wiley.com/10.1002/9781118350553.ch9.

John Maynard Smith and G. R. Price. The Logic of Animal Conflict. *Nature*, 246(5427):15–18, 11 1973. ISSN 0028-0836. doi: 10.1038/246015a0.

A. San Millan, R. Peña-Miller, M. Toll-Riera, Z. V. Halbert, A. R. McLean, B. S. Cooper, and R. C. Maclean. Positive selection and compensatory adaptation interact to stabilize non-transmissible plasmids. *Nature Communications*, 5:1–11, 2014. ISSN 20411723. doi: 10.1038/ncomms6208.

Kareem A. Mosa, Ismail Saadoun, Kundan Kumar, Mohamed Helmy, and Om Parkash Dhankher. Potential Biotechnological Strategies for the Cleanup of Heavy Metals and Metalloids. *Frontiers in Plant Science*, 7 (March):1–14, 3 2016. ISSN 1664-462X. doi: 10.3389/fpls.2016.00303. URL http://journal.frontiersin.org/Article/10.3389/fpls.2016.00303/abstract.

G. Mougabure-Cueto and V. Sfara. The analysis of dose-response curve from bioassays with quantal response: Deterministic or statistical approaches? *Toxicology Letters*, 248:46–51, 4 2016. ISSN 03784274. doi: 10.1016/j.toxlet.2016.03.001. URL http://dx.doi.org/10.1016/j.toxlet.2016.03.001https://linkinghub.elsevier.com/retrieve/pii/S0378427416300376.

Jens Nielsen and Jay D Keasling. Engineering Cellular Metabolism. *Cell*, 164(6):1185–1197, 2016. ISSN 1097-4172. doi: 10.1016/j.cell.2016.02.004. URL http://www.ncbi.nlm.nih.gov/pubmed/26967285.

S. O'Brien, D. J. Hodgson, and A. Buckling. Social evolution of toxic metal bioremediation in Pseudomonas aeruginosa. *Proceedings of the Royal Society B: Biological Sciences*, 281(1787):20140858–20140858, 6 2014. ISSN 0962-8452. doi: 10.1098/rspb.2014.0858. URL http://rspb.royalsocietypublishing.org/content/281/1787/20140858http://rspb.royalsocietypublishing.org/cgi/doi/10.1098/rspb.2014.0858.

Siobhan O'Brien and Michael A. Brockhurst. Social Evolution: Slimy Cheats Pay a Price. *Current Biology*, 25 (9):R378–R381, 2015. ISSN 09609822. doi: 10.1016/j.cub.2015.03.018. URL http://www.sciencedirect.com/science/article/pii/S0960982215003334.

W. F. M. Röling, Michael G. Milner, D. Martin Jones, Kenneth Lee, Fabien Daniel, Richard J P Swannell, and Ian M. Head. Robust Hydrocarbon Degradation and Dynamics of Bacterial Communities during Nutrient-Enhanced Oil Spill Bioremediation. *Applied and Environmental Microbiology*, 68(11):5537–5548, 11 2002. ISSN 0099-2240. doi: 10.1128/AEM.68.11.5537-5548.2002. URL http://aem.asm.org/cgi/doi/10.1128/AEM.68.11.5537-5548.2002.

Peter Rugbjerg, Nils Myling-Petersen, Andreas Porse, Kira Sarup-Lytzen, and Morten O.A. Sommer. Diverse genetic error modes constrain large-scale bio-based production. *Nature Communications*, 9(1), 2018a. ISSN 20411723. doi: 10.1038/s41467-018-03232-w. URL http://dx.doi.org/10.1038/s41467-018-03232-w.

Peter Rugbjerg, Kira Sarup-Lytzen, Mariann Nagy, and Morten Otto Alexander Sommer. Synthetic addiction extends the productive life time of engineered Escherichia coli populations . *Proceedings of the National Academy of Sciences*, 115(10):201718622, 2018b. ISSN 0027-8424. doi: 10.1073/pnas.1718622115.

D. Ryan Georgianna and Stephen P. Mayfield. Exploiting diversity and synthetic biology for the production of algal biofuels. *Nature*, 488(7411):329–335, 2012. ISSN 00280836. doi: 10.1038/nature11479.

M. E. S. Sampah, L. Shen, B. L. Jilek, and R. F. Siliciano. Dose-response curve slope is a missing dimension in the analysis of HIV-1 drug resistance. *Proceedings of the National Academy of Sciences*, 108(18):7613–7618, 2011. ISSN 0027-8424. doi: 10.1073/pnas.1018360108. URL http://www.pnas.org/cgi/doi/10.1073/pnas.1018360108.

Paul A Samuelson. The Pure Theory of Public Expenditure. *The Review of Economics and Statistics*, 36(4):387, 11 1954. ISSN 00346535. doi: 10.2307/1925895. URL https://www.jstor.org/stable/1925895?origin=crossref.

Stefan Schuster, Jan-Ulrich Kreft, Naama Brenner, Frank Wessely, Günter Theißen, Eytan Ruppin, and Anja Schroeter. Cooperation and cheating in microbial exoenzyme production - Theoretical analysis for biotechnological applications. *Biotechnology Journal*, 5(7):751–758, 7 2010. ISSN 18606768. doi: 10.1002/biot.200900303. URL http://doi.wiley.com/10.1002/biot.200900303.

Parker Smith and Martin Schuster. Public goods and cheating in microbes. *Current Biology*, 29(11):R442–R447, 6 2019. ISSN 09609822. doi: 10.1016/j.cub.2019.03.001. URL https://linkinghub.elsevier.com/retrieve/pii/S0960982219302660.

Val H. Smith, David W. Graham, and Dale D. Cleland. Application of resource-ratio theory to hydrocarbon biodegradation. *Environmental Science and Technology*, 32(21):3386–3395, 1998. ISSN 0013936X. doi: 10.1021/es9805019.

Andrew R. Tilman, Joshua Plotkin, and Erol Akçay. Evolutionary games with environmental feedbacks. *bioRxiv*, 2019. doi: 10.1101/493023.

M Vidali. Bioremediation. An overview. *Pure and Applied Chemistry*, 73(7):1163–1172, 7 2001. ISSN 1365-3075. doi: 10.1351/pac200173071163. URL http://www.degruyter.com/view/j/pac.2001.73.issue-7/pac200173071163/pac200173071163.xml.

Joshua S. Weitz, Ceyhun Eksin, Keith Paarporn, Sam P. Brown, and William C. Ratcliff. An oscillating tragedy of the commons in replicator dynamics with game-environment feedback. *Proceedings of the National Academy of Sciences*, 113(47):E7518–E7525, 2016. ISSN 0027-8424. doi: 10.1073/pnas.1604096113. URL http://www.pnas.org/lookup/doi/10.1073/pnas.1604096113.

Stuart A West, Stephen P Diggle, Angus Buckling, Andy Gardner, and Ashleigh S Griffin. The Social Lives of Microbes. *Annual Review of Ecology, Evolution, and Systematics*, 38(1):53–77, 12 2007. ISSN 1543-592X. doi: 10.1146/annurev.ecolsys.38.091206.095740. URL http://www.annualreviews.org/doi/10.1146/annurev.ecolsys.38.091206.095740.